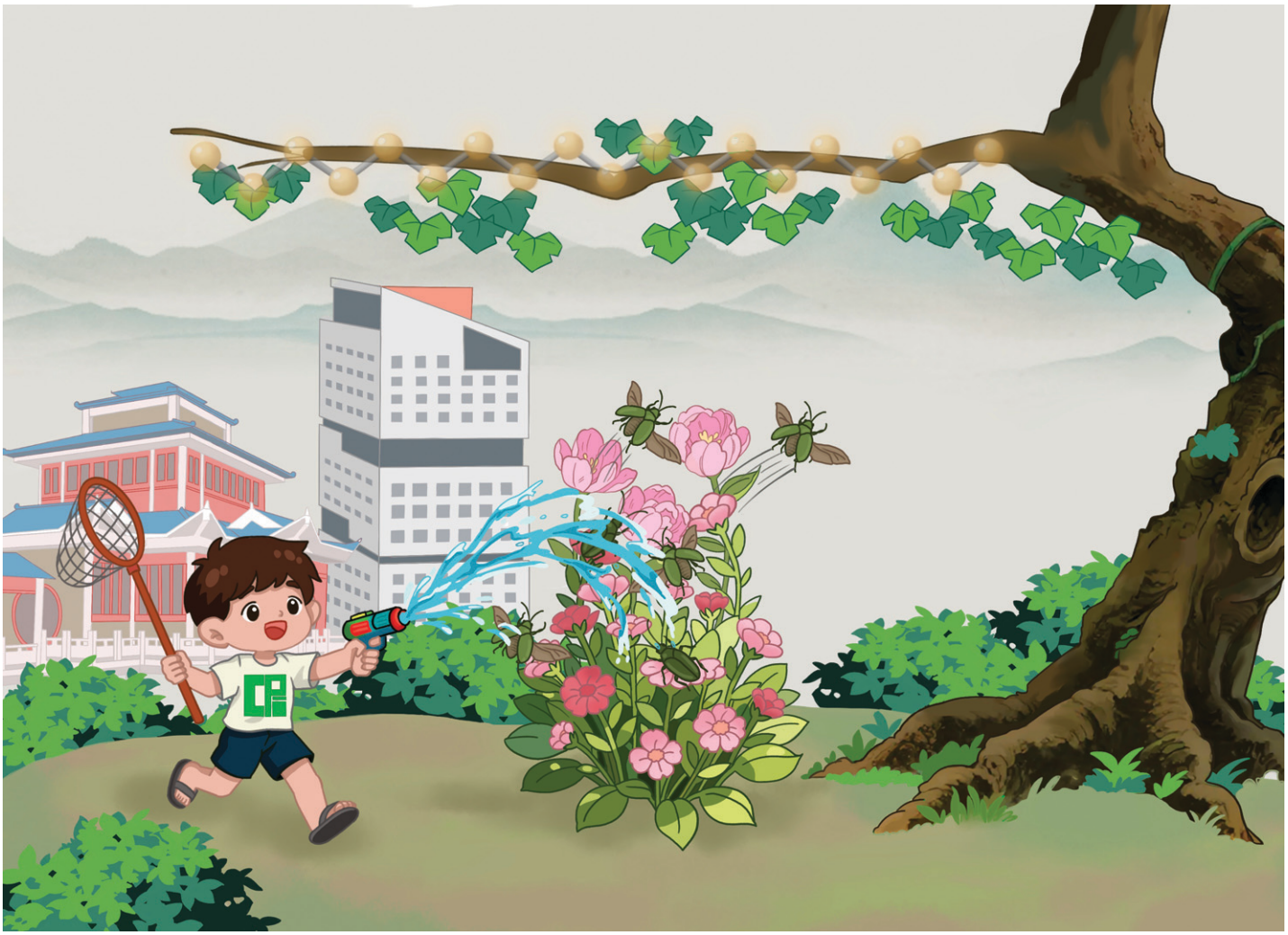

Showcasing research from Ting Qiu's laboratory, Fuzhou University, Fuzhou, China.

Engineering sulfonated polymers for the removal of ultra-trace complexed Cr(III) in tris(2-carboxyethyl) isocyanurate photoresist resin monomers

The concentration of complexed Cr(III) in industrial-grade tris(2-carboxyethyl) isocyanurate can be reduced to meet semiconductor-grade standards through an adsorption–recrystallization process using electron-rich sulfonated polymers.

Image reproduced by permission of Ting Qiu and Jie Chen from *Ind. Chem. Mater.*, 2025, **3**, 618.

As featured in:

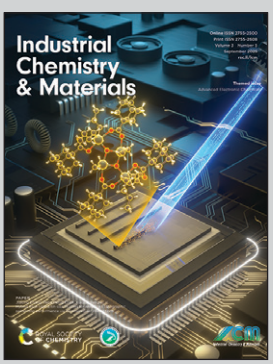

See Ting Qiu, Jie Chen *et al.*, *Ind. Chem. Mater.*, 2025, **3**, 618.

ROYAL SOCIETY OF CHEMISTRY

Industrial Chemistry & Materials

Industrial Chemistry & Materials

ROYAL SOCIETY OF CHEMISTRY

PAPER

View Article Online
View Journal | View Issue

Cite this: *Ind. Chem. Mater.*, 2025, **3**, 618

Engineering sulfonated polymers for the removal of ultra-trace complexed Cr(III) in tris(2-carboxyethyl) isocyanurate photoresist resin monomers†

Huiyao Huang,‡[ab] Shiquan Zhong,‡[ab] Yawen Chen,[a] Wangquan Gong,[a] Changshen Ye,[ab] Ting Qiu *[abc] and Jie Chen *[ab]

The semiconductor manufacturing industry imposes stringent requirements on the metal ion content of photoresist resin monomers. Tris(2-carboxyethyl) isocyanurate (H_3tci), a critical raw material for photoresist resin monomers, inevitably incorporates metal ions during production. However, its inherent carboxyethyl groups form stable coordination complexes with Cr(III), hindering the semiconductor-grade resin monomer production. To achieve the ultra-deep removal of Cr(III) at ultra-trace concentrations, inspired by the hard–soft-acid–base theory, we systematically modulated the electron-rich sulfonic acid group on polymers *via* controlled sulfonation conditions to achieve a novel series of adsorption materials (St) with ultra-high Cr(III) adsorption affinity. The adsorption–recrystallization process using 6 g of St-*V*-15 could reduce the Cr(III) concentration in a solution containing 1 g of H_3tci from 840 ppb to 27.5 ppb. Furthermore, St-*V*-15 exhibited a maximum adsorption capacity of 145 mg g^{-1} calculated using the Langmuir model and a rapid initial adsorption rate of 82.92 mg g^{-1} min^{-1} at 333 K. Additionally, St-*V*-15 demonstrated exceptional selectivity for Cr(III) over competing ions (*e.g.*, K(I), Mg(II), Na(I) and Zn(II)) and maintained stable performance over at least 10 adsorption–desorption cycles. The superior performance originated from the chelation between Cr(III) and the sites of O atoms (S–O and S═O) combined with the electrostatic interaction between deprotonated sulfonic acid groups and Cr(III). These results position St-*V*-15 as a promising adsorption material for ultra-trace Cr(III) removal in H_3tci, offering a cost-effective solution for semiconductor-grade resin monomer production for the very first time.

Keywords: Tris(2-carboxyethyl) isocyanurate; Complexed Cr(III); Ultra-trace; Cr(III) removal; Sulfonated polymers.

Received 14th April 2025,
Accepted 6th June 2025

DOI: 10.1039/d5im00057b

rsc.li/icm

1 Introduction

Photoresist is a critical material in semiconductor fabrication, and its quality directly determines the final performance of semiconductor devices. Photoresist relies on film-forming resins as its core component, which dictates fundamental properties such as lithographic performance and etching resistance.[1] Film-forming resins are typically high-molecular polymers synthesized from resin monomers through chemical reactions like free radical polymerization, copolymerization and esterification.[2,3] During semiconductor device fabrication, the quality of resin monomers directly impacts the chemical properties and application performance of film-forming resins, thereby influencing the manufacturing process level and final yield of semiconductor devices.[4–6] As such, photoresist resin monomers are vital raw materials for semiconductor production.

Among several resin monomers, tris(2-carboxyethyl) isocyanurate (H_3tci) exhibits excellent chemical and thermal stability due to its nitrogen heterocycle structure and multiple carboxylic acid groups, offering broad prospects for applications in film-forming resins.[7,8] However, industrial-grade H_3tci contains metal ion levels that far exceed application requirements, failing to meet relevant technical specifications and quality standards. Meanwhile, the flexible

[a] *College of Chemical Engineering, Fuzhou University, Fuzhou, 350108, China. E-mail: tingqiu@fzu.edu.cn, jiechen@fzu.edu.cn*
[b] *Qingyuan Innovation Laboratory, Quanzhou 362801, P. R. China*
[c] *Fuzhou University International Joint Laboratory of Thermochemical Conversion of Biomass, Fuzhou University, Fuzhou, 350108, China*

† Electronic supplementary information (ESI) available. See DOI: https://doi.org/10.1039/d5im00057b

‡ These authors contributed equally to this work.

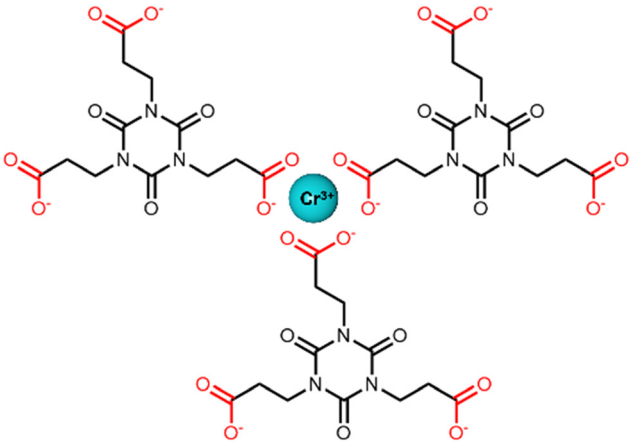

Fig. 1 The Cr(III)–carboxyethyl complexes in H_3tci.

ethyl chains and carboxyl groups in H_3tci form stable Cr(III) complexes (Fig. 1), making it challenging to reduce the level of Cr(III) below 30 ppb using conventional methods such as recrystallization.

Adsorption, with advantages such as designable adsorbents, simple operation and scalability, has emerged as a promising approach for Cr(III) removal in H_3tci.[9–11] To purify H_3tci, the monomer is first dissolved in a solvent, followed by adsorption to remove metal ions and recrystallization to obtain semiconductor-grade monomers.[12] The current adsorbents we have used, such as activated carbon,[13] molecular sieves[14] and polymer gels,[15] only reduce the concentration of Cr(III) to approximately 300 ppb, failing to meet semiconductor standards. This was attributed to the steric hindrance from Cr(III) complexes, which reduces contact between adsorbents and Cr(III), and existing adsorbents rely on weak binding groups such as $–NH_2$, –COOH, and –OH, which cannot compete with carboxyethyl–Cr(III) interactions.[16,17] Meanwhile, there is a low mass transfer efficiency at ultra-trace Cr(III) concentration, coupled with competitive adsorption from H_3tci, limiting affinity and removal efficiency. The core challenge lies in developing dual functional adsorbents capable of both disrupting Cr(III) complexes and providing high affinity for Cr(III).

The sulfonic acid group offers a breakthrough solution due to its unique charge distribution and spatial structure, which enable strong Cr(III) adsorption *via* electrostatic attraction and chelation.[18] The negatively charged species allow positively charged Cr(III) to be electrostatically attracted. Furthermore, the tetrahedral geometry of the sulfonic acid group comprises a S atom bonded to three O atoms, two with double bonds and one carrying a negative charge, which provides an optimal structure for Cr(III) coordination. The negatively charged O atom directly coordinates with Cr(III), while the electron cloud distribution of the sulfonic acid group enhances charge matching and orbital overlap, significantly strengthening binding affinity.[19] Additionally, the deprotonated sulfonic acid group dissociates protons in solvents, which competitively disrupts Cr(III)–carboxyethyl complexes by altering the charge distribution and coordination environment of Cr(III), thereby releasing free Cr(III) for subsequent adsorption. The synergistic mechanism endows sulfonic acid functionalized adsorbents with dual functionality of breaking Cr(III)–carboxyethyl bonds and achieving high affinity adsorption, making them ideal materials for the removal of Cr(III) at ultra-trace concentration in H_3tci.

Among various reported adsorbents, polymers stand out due to their structural stability, ease of processing, low cost, and versatility in functional modification, making them widely applicated in metal ion removal.[20,21] However, the Cr(III) concentration is ultra-trace (approximately 800 ppb) and predominantly exists in complexes in H_3tci. Therefore, achieving deep removal of Cr(III) in H_3tci to below 30 ppb demands an adsorbent with exceptionally high adsorption affinity for Cr(III). While existing sulfonated polymers exhibit promising Cr(III) uptake in the aqueous phase, most research only focuses on adsorption capacity, with little attention given to adsorption affinity.[22,23] To achieve the removal of Cr(III) at ultra-trace concentration in H_3tci, adsorbents must maximize functional group density, as dictated by adsorption equilibrium theory:[24,25] higher group content strengthens affinity, driving equilibrium toward adsorption of Cr(III) and minimizing residual concentrations.

In this work, to achieve high adsorption affinity of sulfonated polymers for Cr(III), we systematically modulated the sulfonation conditions, such as sulfonation time, temperature and sulfuric acid dosage to load varying amounts of sulfonic acid groups, thereby tailoring the adsorption affinity of sulfonated polymers. The sulfonated polymers were applied to the adsorption–recrystallization process of H_3tci, achieving ultra-trace level removal of Cr(III). Further investigations into Cr(III) adsorption behavior included adsorption kinetics and thermodynamics, as well as the impact of H_3tci addition on adsorption performance under competitive coordination conditions. Finally, the adsorption mechanism and cyclic stability were systematically elucidated. This study provides a cost effective and efficient strategy for purifying photoresist resin monomers, addressing critical challenges in semiconductor manufacturing.

2 Results and discussion

2.1 Characterization and structural analysis

The synthesis procedure of sulfonated polymers is shown in Fig. 2a. We first systematically optimized the sulfonation reaction conditions in the order of reaction time, temperature and sulfuric acid dosage. The polymers with different sulfonation times were named St-*t*-*x* (h), those with different sulfonation temperatures were marked as St-*T*-*x* (°C) and those with different dosages of sulfuric acid were named St-*V*-*x* (mL).

The successful synthesis of St and subsequent sulfonation were verified through Fourier transform infrared (FTIR)

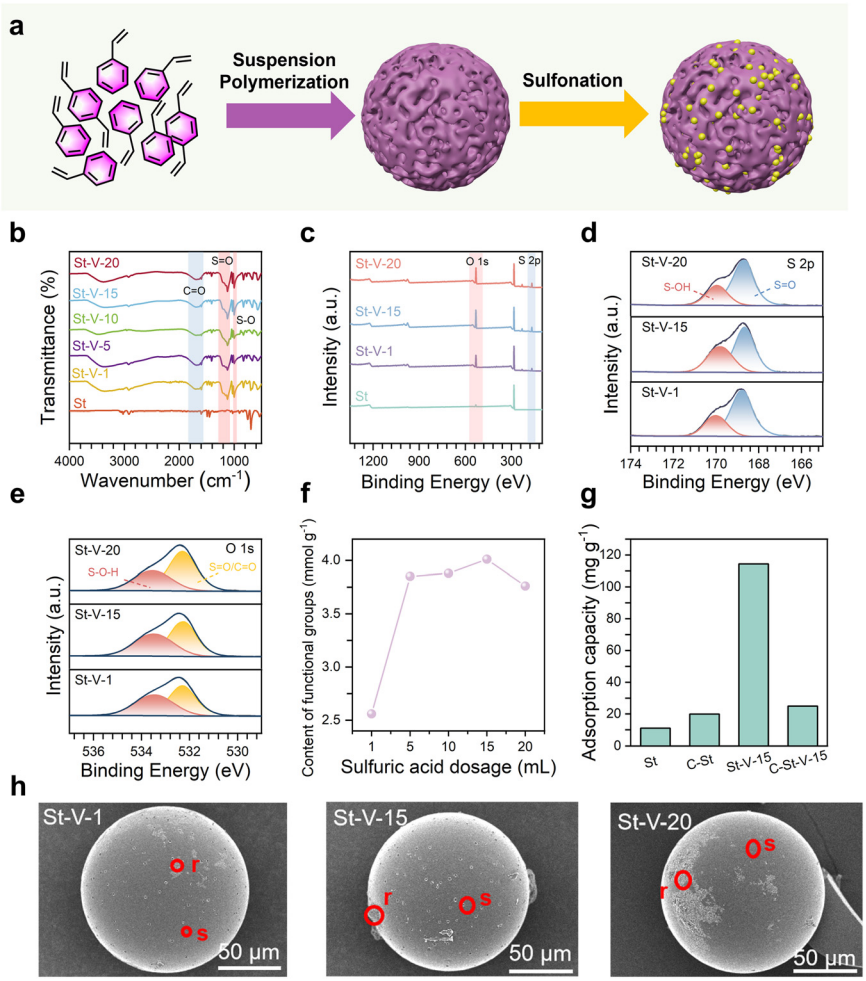

Fig. 2 (a) Synthesis scheme of sulfonated polymers; (b) FTIR spectra; (c) XPS full scan spectra; (d) S 2p spectra; (e) O 1s spectra; (f) content of sulfonic acid groups of St-*V*-*x*; (g) adsorption capacity of sulfonated polymers before and after calcination; (h) SEM images of St-*V*-*x*.

analysis (Fig. 2b and S1–S2†). The peak at 3026 cm^{-1} corresponded to the C–H stretching vibration, while the peak at 2918 cm^{-1} could be attributed to the abundant $-CH_2$ groups in the polymer backbone. The characteristic peaks in the range of 1410 cm^{-1} to 1603 cm^{-1} arose from the stretching vibrations of C=C bonds in the benzene rings. After sulfonation, the above peaks of all sulfonated polymers remained intact, indicating that the sulfonation process did not compromise the skeletal structure of St. Notably, two new characteristic peaks emerged at 1121 cm^{-1} and 1030 cm^{-1}, which were assigned to the S=O and S–O stretching vibrations, respectively, indicating the successful grafting of the sulfonic acid group.[26] In addition to the FTIR results, a new peak corresponding to S 2p at 168.6 eV was observed in the X-ray photoelectron spectra (XPS) (Fig. 2c), confirming the successful introduction of sulfur related groups. Further analysis of the S 2p spectra revealed peaks at 169.90 eV and 168.68 eV (Fig. 2d), corresponding to S=O and S–O bonds, respectively. Meanwhile, the O 1s spectra exhibited peaks at positions 533.50 eV and 532.25 eV (Fig. 2e), assigned to S=O/C=O and S–O bonds, respectively.[27] These findings conclusively demonstrate the successful sulfonation of St.

Interestingly, as the sulfonation time, temperature and sulfuric acid dosage increased, the intensities of the S=O and S–O peaks initially increased and then decreased, indicating that the content of sulfonic acid groups on the sulfonation polymers firstly rose and subsequently decreased with prolonged sulfonation time, elevated temperature and excessive sulfuric acid dosage. This phenomenon might be attributed to the carbonization process happened during the reaction of sulfuric acid with polymers, which could lead to dehydration of sulfonic acid groups on the polymer surface, resulting in the formation of other functional groups. To investigate the reason for the tendency of the peak intensities of S–O and S=O, the sulfonic acid group contents of sulfonated polymers were quantified *via* titration (Fig. 2f and S3–S4†). It could be observed that the trend in the content of sulfonic acid groups in sulfonated polymers, as influenced by sulfonation conditions, aligns with that observed in the FTIR spectra. Specifically, too harsh sulfonation conditions lead to a decrease in the content of sulfonic acid groups. Scanning

electron microscopy (SEM) images of the sulfonated polymers are shown in Fig. 2h and S5 and S6.† With increasing time, temperature and sulfonic acid dosage, the surface of sulfonated polymers became progressively rougher, which likely hindered sulfonic acid group grafting and then reduced content. Notably, all sulfonated polymers exhibited a spherical bead morphology, indicating that no additional shaping is required for subsequent processing, enabling direct industrial use. To explore the origin of roughness, energy dispersive spectrometry (EDS) point scans were performed on rough (designated as St-*y*-*x*-r) and smooth (St-*y*-*x*-s) regions of the surface of sulfonated polymers (Table 1 and S1†). Taking St-*V*-*x* as an example, the results showed that compared with St-*V*-*x*-s, St-*V*-*x*-r had higher carbon (C) and oxygen (O) contents but lower sulfur (S) content. This phenomenon was attributed to carbonization of the polymer surface induced by excessive sulfuric acid, which impeded the grafting of sulfonic acid groups.[28] Furthermore, the carbonization degree induced by excessive sulfuric acid dosage was less severe compared to that caused by harsher sulfonation time and temperature. This phenomenon may be attributed to the increased thermal energy input associated with elevated temperatures and prolonged times, which thereby intensifies dehydrogenation reactions and crosslinking reactions, ultimately leading to a higher degree of carbonization.

2.2 The effect of carbonization

To investigate the impact of carbonization on the adsorption performance of the sulfonated polymers, we calcined St and St-*V*-15 at 300 °C for 1 h to achieve complete carbonization, labeling them C-St and C-St-*V*-15, respectively. A comparison of their FTIR spectra revealed that both polymers retained characteristic peaks of polymers (Fig. S7†), indicating that the carbonization did not significantly disrupt the polystyrene skeleton, demonstrating excellent structural stability. However, the peaks of S–O at 1030 cm^{-1} and 829 cm^{-1} and O–H at 3395 cm^{-1} disappeared, while the intensity of the S=O stretching vibration peak at 1121 cm^{-1} markedly decreased.[29] Concurrently, the S and O contents in C-St-*V*-15 significantly dropped, indicating the elimination of most sulfonic acid groups during carbonization. Interestingly, the specific surface areas of St and St-*V*-15 increased from 0.5665 $m^2 g^{-1}$ and 0.1456 $m^2 g^{-1}$ to 0.7082 $m^2 g^{-1}$ and 0.2298 $m^2 g^{-1}$ after carbonization, respectively. This enhancement was attributed to the thermal decomposition of unstable components in the polymer during high-temperature treatment, which generated gas release and subsequent pore formation.

To evaluate their maximum adsorption capacity, experiments were conducted using a 200 ppm Cr(III) solution. Due to the increased specific surface area, the maximum adsorption capacity of carbonized St rose from 11.1 mg g^{-1} to 19.9 mg g^{-1}. In contrast, the carbonized St-*V*-15 exhibited a drastic decline in adsorption capacity from 114.3 mg g^{-1} to 25.0 mg g^{-1}, primarily due to the removal of most sulfonic acid groups during carbonization. This once again strongly demonstrated the crucial role played by sulfonic acid groups in the adsorption of Cr(III).

2.3 The relationship between the sulfonic acid group content and the adsorption affinity

A positive correlation existed between the distribution coefficient (K_d) and adsorption affinity, and elevated K_d values reflected stronger adsorption affinity. To investigate the relationship between the sulfonic acid group content and adsorption affinity, the sulfonic acid group contents of sulfonated polymers were quantified *via* titration, and their adsorption performance was evaluated using a 10 ppm Cr(III) solution. As shown in Fig. 3a–c, the K_d values for Cr(III) adsorption of sulfonated polymers were not constant but dynamically changed in response to variations in sulfonic acid group loading. The data demonstrated a significant positive correlation between these two parameters. Specifically, the K_d value steadily increased with rising sulfonic acid group loading, while a decrease in sulfonic acid group loading led to a corresponding decline in K_d. This strong correlation suggested that the adsorption affinity of sulfonated polymers for Cr(III) was predominantly determined by sulfonic acid group loading rather than being affected by multiple complex factors. This mechanism arises because sulfonic acid groups serve as critical active sites during adsorption, where their quantity directly determines both the probability and intensity of interactions with Cr(III). Higher loading provided more active sites, enhanced attraction forces with Cr(III), promoted greater Cr(III) adsorption onto polymer surfaces, and consequently raised K_d values and strengthened adsorption affinity. Conversely, reduced loading diminishes these effects and weakens adsorption affinity. Notably, St-*V*-15 exhibited the highest sulfonic acid group

Table 1 The EDS point scan results of St-*V*-*x*

Sample	C (wt%)	C (wt% Sigma)	O (wt%)	O (wt% Sigma)	S (wt%)	S (wt% Sigma)
St-*V*-1-r	73.02	0.24	12.66	0.21	14.32	0.12
St-*V*-1-s	69.80	0.32	7.26	0.22	22.93	0.23
St-*V*-15-r	68.07	0.22	22.59	0.21	9.34	0.07
St-*V*-15-s	55.18	0.49	8.88	0.23	35.94	0.39
St-*V*-20-r	68.10	0.22	18.44	0.20	13.46	0.10
St-*V*-20-s	63.86	0.25	22.03	0.22	14.11	0.10

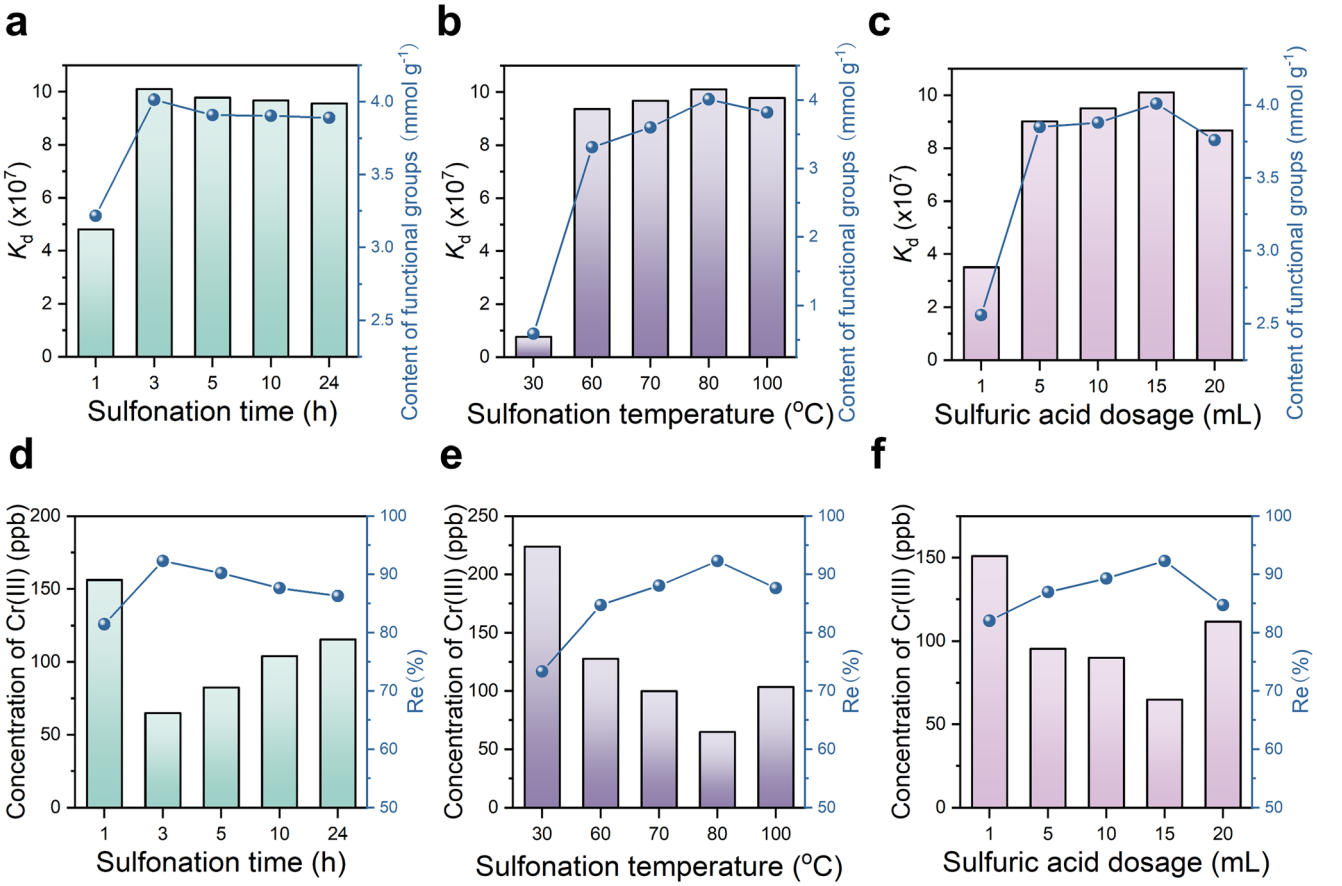

Fig. 3 Relationship between K_d values and sulfonic acid group content of (a) St-*t*-*x*, (b) St-*T*-*x* and (c) St-*V*-*x*; the adsorption–recrystallization process results of (d) St-*t*-*x*, (e) St-*T*-*x* and (f) St-*V*-*x*.

content of 4.01 mmol g^{-1} and the maximum K_d value of 10.1 × 10^7 mL g^{-1}, which is significantly higher than those of other reported materials, such as PSSC (0.21 × 10^6 mL g^{-1}),[30] hPAN/PVPI/GO (0.72 × 10^6 mL g^{-1})[31] and APTES (0.11 × 10^6 mL g^{-1}).[32] Generally, a K_d value exceeding 10^4 mL g^{-1} was sufficient to demonstrate the exceptional adsorption affinity for the target adsorbate, underscoring the exceptional performance of St-*V*-15 in Cr(III) removal.[33]

Building on the excellent Cr(III) adsorption affinity, we applied the sulfonated polymers to a H_3tci adsorption–recrystallization process, and the results are shown in Fig. 3d–f. ICP-MS analysis revealed that the 1 g initial Cr(III) concentration in H_3tci dissolved in water was 840 ppb. However, recrystallization alone without adsorption only reduced the Cr(III) concentration to 441.7 ppb, achieving a removal efficiency of 47.42%. In contrast, when 2 g of sulfonated polymers were employed for adsorption prior to recrystallization, all sulfonated polymers achieved Cr(III) removal efficiencies exceeding 70%. Notably, St-*V*-15 reduced the Cr(III) concentration in H_3tci from 840 ppb to 67.6 ppb, with a removal efficiency as high as 92.29%, significantly outperforming all commercial adsorbents we have used under the same conditions (Fig. S8†). Furthermore, as the parameters of sulfonation (time, temperature and sulfuric acid dosage) increased, the Cr(III) removal efficiency of sulfonated polymers initially improved and then decreased, aligning with the trends in the sulfonic acid group content and distribution coefficients. This evidence strongly supported that the removal of complexed Cr(III) from H_3tci was primarily governed by the sulfonic acid group content, a

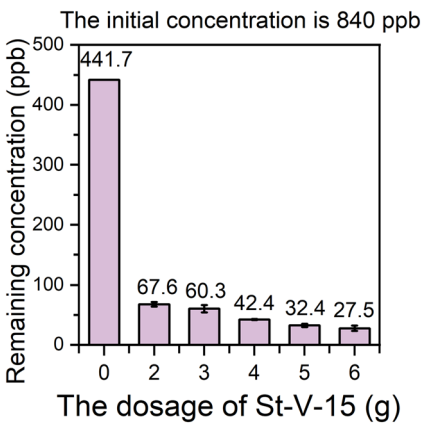

Fig. 4 The influence of the dosage amount of St-*V*-15 on the adsorption–recrystallization process.

finding that provided critical guidance for the rational design of future materials.

2.4 The influence of the adsorbent dosage on purification of Cr(III) in H_3tci

When investigating the relationship between the sulfonic acid content and practical Cr(III) efficiency in H_3tci, St-*V*-15 could reduce the Cr(III) concentration from 840 ppb to 67.6 ppb, which still fell short of semiconductor-grade standards. To address this, we further increased the dosage of St-*V*-15, ultimately achieving semiconductor-grade Cr(III) levels in H_3tci, as demonstrated in Fig. 4. It was observed that as the dosage of St-*V*-15 increased, the remaining concentration of Cr(III) progressively decreased. Notably, when the dosage reached 6 g, the remaining concentration of Cr(III) in H_3tci dropped to 27.5 ppb, which demonstrated that St-*V*-15 could achieve ultra-trace removal of Cr(III) in the production process of semiconductor-grade H_3tci, fulfilling the stringent purity requirements for advanced lithography applications.

2.5 Adsorption isotherms

To further elucidate the influence of sulfonic acid group loading on the maximum adsorption capacity of Cr(III) and related thermodynamic parameters, adsorption isotherm experiments were conducted for St-*V*-*x* at 298 K, 313 K and 333 K with initial Cr(III) concentration ranging from 10 to 400 ppm. As shown in Fig. 5a, the adsorption isotherms at all three temperatures exhibited the characteristics of type I behavior, indicating strong interactions between the sulfonated polymer and Cr(III).[34] This demonstrated the potential of the sulfonated polymer to remove Cr(III) at ultra-trace concentration. Furthermore, as the adsorption temperature increased, the adsorption capacities of the series of sulfonated polymers increased accordingly, indicating that the adsorption of Cr(III) by the sulfonated polymer was an endothermic process, and higher temperatures were conducive to the adsorption process.

Meanwhile, the Langmuir and Freundlich adsorption isotherm models were employed to describe the interactions between the sulfonated polymer and Cr(III), as illustrated in Fig. 5b and c and S9,† with corresponding parameters listed in Table S2.† The results indicated that sulfonated polymers exhibited higher fitting accuracy to the Langmuir model at all three temperatures, and the correlation coefficients (R^2) all exceeded 0.99, which suggested that the Langmuir model was more suitable for describing the adsorption behavior of Cr(III) on the sulfonated polymer, implying a monolayer adsorption process.[35] The equilibrium constant (K_L) derived from the Langmuir model also exhibited the same trend as the sulfonic group content, further indicating that higher group content corresponded to stronger adsorption affinity. Notably, the maximum adsorption of St-*V*-15 calculated using the Langmuir model reached a remarkable 126 mg g^{-1} at 298 K, which was higher than that of Fh (22.93 mg g^{-1}),[36] Ti-4BC (112.4 mg g^{-1}),[37] COF@SO_3H (105.26 mg g^{-1}),[18] *etc.*

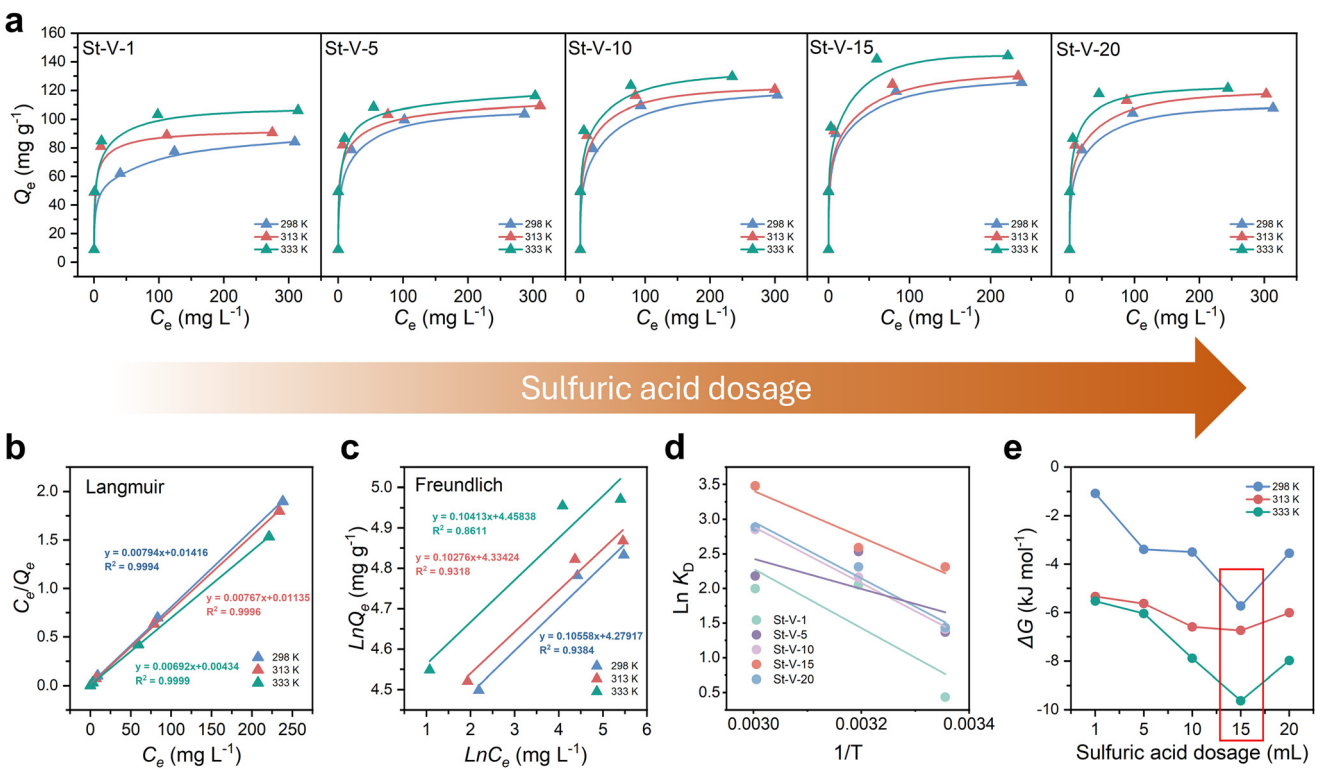

Fig. 5 (a) Adsorption isotherms of St-*V*-*x*; (b) Langmuir model and (c) Freundlich model of St-*V*-15; (d) adsorption thermodynamic fitting diagram and (e) ΔG diagram of St-*V*-*x*.

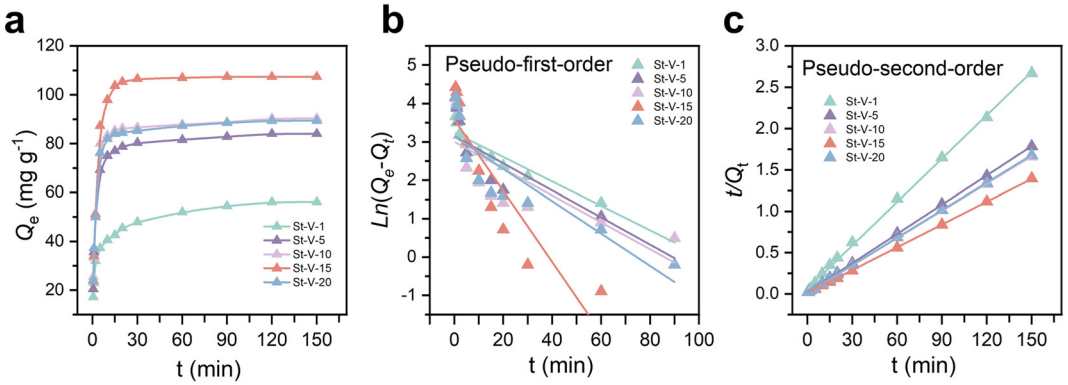

Fig. 6 (a) Adsorption kinetics, (b) pseudo-first-order model and (c) pseudo-second-order model of St-*V*-*x*.

Thermodynamic studies were conducted on sulfonated polymers with varying sulfuric acid dosages to further analyze the influence of the functional group content on the Cr(III) adsorption affinity, and the results are shown in Fig. 5d and Table S3.† All sulfonated polymers exhibited positive ΔH values, strongly confirming that Cr(III) adsorption was an endothermic process and higher temperatures favored the adsorption process.[38] Additionally, the positive ΔS values indicated an increase in system disorder during adsorption. Furthermore, the calculated ΔG values at all temperatures were negative, demonstrating the spontaneity of Cr(III) adsorption on the sulfonated polymers.[39] Notably, the ΔG values became more negative with rising temperature, confirming enhanced adsorption affinity at higher temperatures (Fig. 5e). Further comparison of ΔG values of St-*V*-*x* polymers revealed that at all temperatures, the ΔG values became more negative with increasing sulfonic acid group content, further underscoring the strong positive correlation between the sulfonic acid group loading and adsorption affinity.

2.6 Adsorption kinetics

The adsorption rate is a critical parameter for evaluating adsorbent materials. To this end, we first investigated the adsorption kinetics of St-*V*-*x* in an aqueous system with a 200 ppm Cr(III) concentration, and the results are shown in Fig. 6a. The steep slopes of the adsorption capacity *versus* time curves of St-*V*-*x* with varying sulfuric acid group contents indicated excellent adsorption rates and affinity for Cr(III). The adsorption rates of sulfonated polymers with different sulfuric acid group loadings exhibited consistent trends as the sulfuric acid dosage varied, strongly suggesting that sulfonic acid groups played a dominant role in Cr(III) adsorption. Notably, St-*V*-15 achieved nearly its equilibrium adsorption capacity within 30 min, reaching an exceptional adsorption capacity of 107.42 mg g^{-1} at equilibrium.

Subsequently, the kinetic data were fitted using the pseudo-first-order and pseudo-second-order kinetic models, and the results are presented in Fig. 6b and c and Table S4.† The pseudo-second-order model provided a correlation coefficient (R^2) exceeding 0.999 for all St-*V*-*x*, far surpassing those of the pseudo-first-order model. This confirmed that the adsorption process was dominated by chemisorption, further emphasizing the pivotal role of sulfonic acid groups.[40,41] Furthermore, the initial adsorption rates ($h = K_2 Q_e^2$) exhibited a trend consistent with the sulfonic acid group content. Remarkably, St-*V*-15 demonstrated an exceptional h of 82.92 mg g^{-1} min^{-1}, highlighting its superior affinity for Cr(III).

2.7 The influence of H_3tci during the adsorption process

To gain deeper insights into the adsorption behavior of sulfonated polymers for Cr(III) in the presence of competing coordination by H_3tci, we conducted adsorption isotherm and kinetic experiments by adding 1 g L^{-1} H_3tci to the Cr(III) solution (Fig. 7a and b). After the addition of H_3tci, the initial slopes of the adsorption isotherm curves at all three temperatures decreased compared to the system without H_3tci, and the adsorption capacities were reduced to a certain extent. However, the adsorption behavior remained consistent with the Langmuir model (Fig. S10 and Table S5†), although the calculated maximum adsorption capacity decreased by approximately 30 mg g^{-1} across all conditions, and the equilibrium constants (K_L) reflecting surface affinity also decreased significantly. Comparative analysis of adsorption thermodynamic data revealed that the addition of

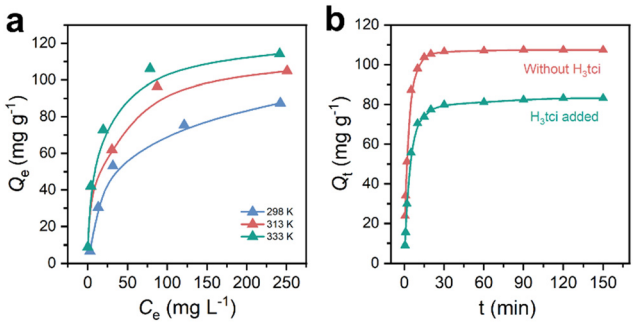

Fig. 7 (a) Adsorption isotherms and (b) adsorption kinetics of St-*V*-15 in a H_3tci-containing Cr(III) solution.

H_3tci to the Cr(III) solution resulted in decreased ΔH and ΔS values, alongside increased ΔG (Fig. S11†). In kinetic experiments, the slopes of the curves with H_3tci addition were notably lower, and the adsorption capacity at equilibrium decreased from 107.42 mg g^{-1} to 83.23 mg g^{-1}. Nevertheless, the adsorption behavior of St-*V*-15 still conformed to the pseudo-second-order model (Fig. S12 and Table S6†), albeit with a marked reduction in the initial adsorption rate h from 82.92 mg g^{-1} min^{-1} to 28.65 mg g^{-1} min^{-1}. The Weber–Morris model was applied to describe the intraparticle diffusion process, and the results are shown in Fig. S13 and Table S7.† It could be observed that in both H_3tci-added and H_3tci-free systems, the diffusion behavior of Cr(III) in St-*V*-15 involved three stages: liquid film diffusion, intraparticle diffusion and equilibrium stages. In the first stage, the fitted curves did not pass through the origin of the plot, indicating that liquid film diffusion was not the sole rate-limiting step. During the intraparticle diffusion stage, the k_2 value remained as high as 5.30 mg g $min^{-0.5}$ even in the presence of H_3tci, demonstrating rapid Cr(III) diffusion within the St-*V*-15 particle. These results indicated that the introduction of H_3tci induced competitive interactions between the carboxyl groups and Cr(III), leading to reduced adsorption affinity of St-*V*-15 for Cr(III), but did not alter the fundamental adsorption mechanism.

2.8 Selective adsorption

To further investigate the potential of the adsorbent for selective Cr(III) capture and evaluate its anti-interference capability in practical H_3tci-containing systems, the sulfonated polymer St-*V*-15 was tested for Cr(III) adsorption selectivity in a mixed metal solution containing five coexisting ions (Cr(III), K(I), Mg(II), Na(I) and Zn(II)) at an initial concentration of 100 ppm for each metal ion. As depicted in Fig. 8a, St-*V*-15 demonstrated exceptional selectivity for Cr(III) with negligible adsorption of the other metal ions. Specifically, the adsorption capacity of St-*V*-15 for Cr(III) reached 68.2 mg g^{-1}, while for the other metals, the maximum adsorption was only 3.2 mg g^{-1}, which was attributed to the higher charge density of Cr(III), enabling stronger electrostatic interactions with sulfonic acid groups. Meanwhile, combined with the concentration of the other metal ions in H_3tci before and after adsorption–recrystallization (Table S8†), it could be observed that the concentration of the other metal ions exhibited a slight reduction, which could be attributed to the removal of metal ions by recrystallization. The selective adsorption experiment indicated that St-*V*-15 exhibited strong anti-interference capability in Cr(III) adsorption.

2.9 The effect of pH

The surface chemical properties of the adsorbent and the speciation of Cr(III) are highly pH dependent. Cr species primarily exist as Cr(III) at a pH of 1.0–4.0 and as $Cr(OH)_2^+$ and $Cr(OH)^{2+}$ at a pH of 4.0–6.0 and precipitate as $Cr(OH)_3$ at a pH exceeding 6.0.[42] To investigate pH effects, adsorption experiments were conducted using the sulfonated polymer for a 100 ppm Cr(III) solution adjusted to pH 1.0, 3.5, and 5.0 with 1 M HCl or 1 M NaOH and the point of zero charge (pH_{pzc}) of St-*V*-15 was determined to be 3.67 through zeta potential measurement. As shown in Fig. 8b and c, the St-*V*-*x* series exhibited the highest adsorption capacity at a pH of 5.0. At the pH of 1.0 and 3.5 ($pH > pH_{pzc}$), the surface of sulfonated polymers was protonated due to the high concentration of H^+, while Cr species predominantly existed as Cr(III). The electrostatic repulsion between positively charged polymer surfaces and Cr(III) ions led to reduced adsorption. When the pH was adjusted to 5.0 ($pH < pH_{pzc}$), the surface became deprotonated, carrying a negative charge. Concurrently, Cr(III) existed as hydrolyzed species. The electrostatic attraction between the negatively charged polymer and positively charged Cr(III) hydroxo-complex enhanced adsorption capacity. Notably, as shown in Fig. S14,† a turbid solution formed when the pH exceeded 5.5. Additionally, the equivalent amount of G3-grade TMAH or HNO_3 was added to investigate the effect of pH on the adsorption–recrystallization and the results are shown in Fig. S15.† It was observed that the removal efficiency of Cr(III) in H_3tci was enhanced under alkaline conditions, which could be attributed to both H^+ and OH^- ions disrupting the complexation between Cr(III) and H_3tci. Under acidic conditions, the sulfonic acid groups existed as $-SO_3H$,

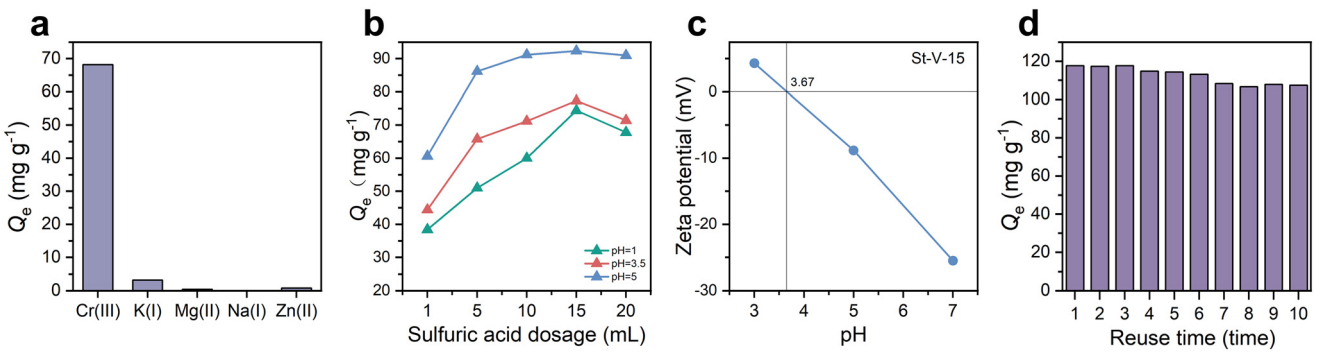

Fig. 8 (a) Adsorption selectivity of St-*V*-15; (b) effect of pH, (c) zeta potential and (d) reuse time of St-*V*-15.

exerting electrostatic repulsion against Cr(III), whereas under alkaline conditions, they transformed into $-SO_3^-$, enabling electrostatic attraction to Cr(III).

2.10 Reusability

The ability of an adsorbent to maintain its structural integrity and adsorption performance during desorption–regeneration and repeated use is a critical indicator for evaluating economic viability and practical applicability. Therefore, to investigate the stable recyclability of sulfonated polymer St-*V*-15, ten consecutive adsorption and desorption cycles were conducted using a 20 wt% sulfuric acid solution as the desorption agent for Cr(III) removal from an initial 200 ppm Cr(III) solution. As shown in Fig. 8d, the adsorption capacity of St-*V*-15 for Cr(III) decreased by only 9% after ten cycles, which may be caused by the incomplete Cr(III) removal during desorption. In summary, St-*V*-15 exhibited stable and efficient regeneration capability.

2.11 Adsorption mechanism

To delve deeper into the adsorption mechanism between the sulfonated polymer and Cr(III), we characterized St-*V*-15 before and after the adsorption experiment using FTIR and XPS, with the post-adsorption material marked as St-*V*-15-Cr. It could be observed that after Cr(III) adsorption, the intensity of the peak referring to the O–H bond in $-SO_3H$ at 3395 cm^{-1} decreased, while the original peak at 1120 cm^{-1} split into a doublet (Fig. 9a).[43] This phenomenon was caused by the O atoms in $-SO_3H$ possessing lone pair electrons, which coordinate with Cr(III) and alter the electron cloud distribution of $-SO_3H$. The XPS survey spectrum of St-*V*-15-Cr exhibited a new peak corresponding to Cr 2p at 577.69 eV and the weakened S 2p signal at 169.57 eV was attributed to surface signal masking by Cr(III) (Fig. 9b), further confirming successful Cr(III) adsorption. Further comparison of the O 1s and S 2p XPS spectra of St-*V*-15 before and after Cr(III) adsorption revealed significant peak shifts (Fig. 9c and d). For the O 1s spectra, the peaks assigned to S–O and S═O bonds shifted from 533.49 eV and 532.21 eV to 533.12 eV and 531.92 eV, respectively. Similarly, the peaks corresponding to S–O and S═O bonds shifted from 169.91 eV and 168.76 eV to 169.58 eV and 168.40 eV in the S 2p spectra, respectively. These shifts provided compelling evidence for chelation between Cr(III) and the sites of O atom (S═O and S–O) on the sulfonic groups, which combined with the electrostatic interaction between deprotonated sulfonic acid groups and Cr(III) as mentioned in section 2.9, as summarized in Fig. 10.

3 Conclusions

In summary, by systematically optimizing sulfonation conditions, the sulfonic acid group content on the polymer was tailored, and St-*V*-15 showed a high sulfonic acid group content of 4.01 mmol g^{-1} and achieved a distribution coefficient (K_d) of 10.1 × 10^7 mL g^{-1} in a 10 ppm Cr(III) solution, demonstrating exceptional adsorption affinity for Cr(III). Furthermore, St-*V*-15 exhibited a maximum Langmuir adsorption capacity of 145 mg g^{-1}, a rapid initial adsorption rate of 82.92 mg g^{-1} min^{-1}, outstanding selectivity for Cr(III) and remarkable reusability. When applied to H_3tci purification by adsorption–recrystallization, 6 g of St-*V*-15 could reduce the Cr(III) level from 840 ppb to 27.5 ppb in a solution containing 1 g of H_3tci, meeting stringent semiconductor-grade standards. Mechanistic studies have found that its interaction with Cr(III) mainly occurred through synergistic chelation of the O atom in S–O/S═O and electrostatic interactions with deprotonated sulfonic acid groups. This study demonstrated the sulfonated polymer St-*V*-15 as an exceptional adsorbent for ultra-trace Cr(III) removal in H_3tci, addressing critical purity requirements for semiconductor manufacturing.

4 Experimental section

4.1 Chemicals

Methanol, ethanol, *N*,*N*-dimethylformamide, sodium chloride, hydrochloric acid, sodium hydroxide, dichloroethane, sulfuric acid, acetone, zinc nitrate hexahydrate, potassium nitrate, sodium nitrate, and nitric acid were acquired from Sinopharm Chemical Reagent Co., Ltd. Polyvinyl alcohol, styrene, divinylbenzene and

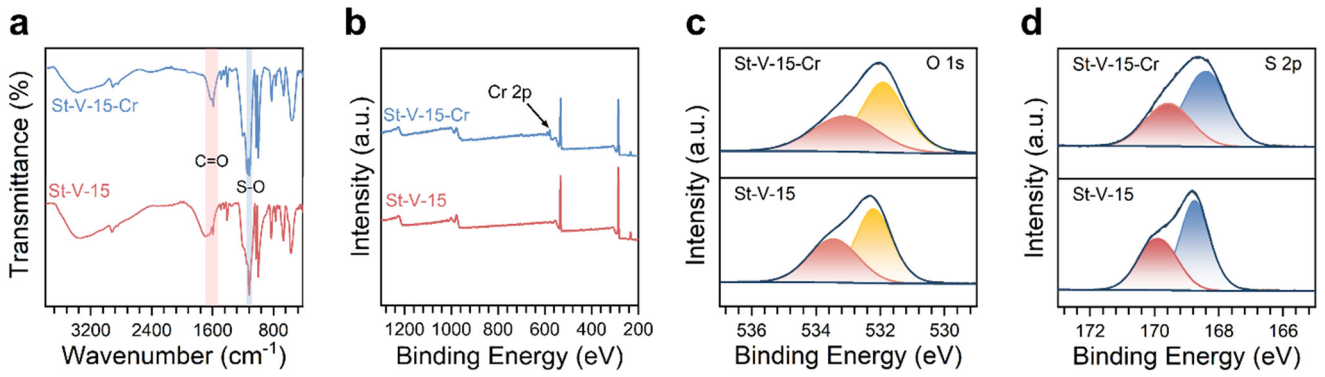

Fig. 9 (a) FTIR spectra, (b) XPS full scan, (c) O 1s spectra and (d) S 2p spectra of St-*V*-15 and St-*V*-15-Cr.

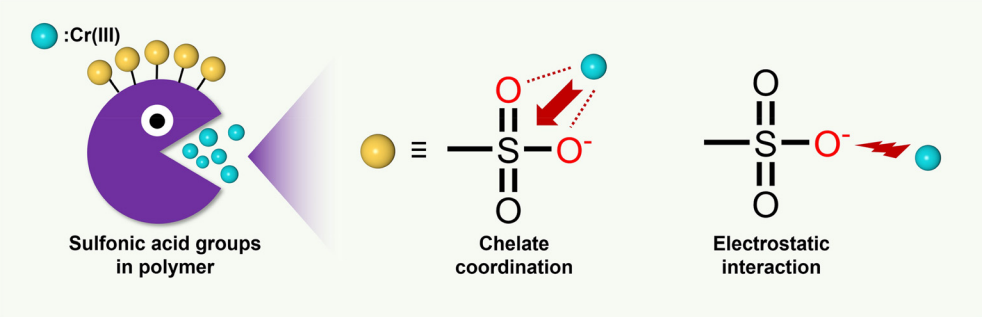

Fig. 10 The proposed mechanism of St-*V*-15 adsorbing Cr(III).

2,2-azobisisobutyronitrile were purchased from Shanghai Macklin Biochemical Technology Co., Ltd. Chromium nitrate nonahydrate was supplied by Shanghai Aladdin Biochemical Technology Co., Ltd, and tris(2-carboxyethyl) isocyanurate was produced by Tianjin Fuyu Fine Chemical Co., Ltd. All reagents were of AR grade and were used without further purification. The water used was prepared in the laboratory with a resistivity of 18 MΩ cm.

4.2 Synthesis of sulfonated polymers

St was synthesized *via* suspension polymerization. Initially, 0.1 g of polyvinyl alcohol and 2.0 g of sodium chloride were dissolved in 100 mL of water, and the aqueous phase was prepared by stirring at 65 °C for 1 h. Next, 0.84 mL of divinylbenzene (DVB), 7.6 mL of styrene monomer, and 0.12 g of 2,2′-azobisisobutyronitrile (AIBN) were ultrasonically mixed to form the oil phase. The oil phase was injected into the aqueous phase using a constant-flow pump, followed by mechanical stirring at 65 °C for 2 h. The temperature was then gradually increased to 75 °C, 85 °C and 90 °C, maintaining at 75 °C for 2 h, 85 °C for 2 h and 90 °C for 30 min, respectively, to promote polymerization. After cooling, the liquid phase was removed by filtration, and the product was alternately washed with water and methanol three times. The microspheres were then stirred overnight in 100 mL of DMF at room temperature. Finally, the liquid phase was removed by filtration, and the product was washed with water and methanol three times again and dried at 60 °C for 24 h.

20 mL of 1,2-dichloroethane as a swelling agent was added to 1.0 g of St, and the mixture was stirred at 60 °C and 100 rpm for 0.5 h to allow swelling. Subsequently, we slowly added concentrated sulfuric acid (in amounts of 1 mL, 5 mL, 10 mL, 15 mL and 20 mL, respectively) and raised the temperature to a specific value (30 °C, 60 °C, 70 °C, 80 °C and 100 °C, respectively) for sulfonation, with reaction times of 1 h, 3 h, 5 h, 10 h and 24 h, respectively. After sulfonation, the liquid phase was removed by filtration, and the product was alternately washed with water and ethanol until neutral, and then stirred overnight with acetone to remove 1,2-dichloroethane. Finally, the liquid phase was removed by filtration, and the product was washed with water and ethanol three times again and dried at 60 °C for 24 h.

4.3 Characterization

Fourier transform infrared (FTIR) spectroscopy was performed using a Nicolet iS50 spectrometer with a scanning range of 400–4000 cm^{-1}. Elemental analysis (EA) was conducted on a Vario EL Cube analyzer. N_2 adsorption–desorption isotherms were measured using an ASAP 2460 analyzer. Scanning electron microscopy (SEM) images were acquired with a Regulus 8100 microscope. X-ray photoelectron spectroscopy (XPS) data were collected using an EscaLab 250Xi spectrometer.

4.4 Determination of sulfonic acid group content

25 mL of sulfonated polymers were loaded into a glass column and washed with deionized water until the effluent was clear and free of visible impurities. 400 mL of 1 M HCl solution was passed through the column at 14 mL min^{-1}, followed by rinsing with deionized water for 30 min at 14 mL min^{-1}. Subsequently, 400 mL of 1 M NaCl solution was passed through the column at 14 mL min^{-1} to convert all functional groups to the sodium form. The polymer was then rinsed with deionized water until the effluent remained colorless upon addition of phenolphthalein.

Two portions of sodium-form sulfonated polymers (1 g each) were loaded into glass columns, followed by the addition of 5 mL deionized water. 150 mL of 1 M HCl solution was passed through each column at 4 mL min^{-1}. The effluent was discarded, and the polymer was rinsed with 20 mL deionized water at 4 mL min^{-1} until the effluent turned yellow upon testing with a methyl orange indicator. 100 mL of 1 M NaCl solution was passed through the sulfonated polymer at 2 mL min^{-1} and collected in a 250 mL conical flask. One drop of phenolphthalein indicator was added to the collected eluent, which was then titrated with 0.1 M NaOH solution until a faint pink color persisted for 15 s.

$$Q = \frac{(V_1 - V_2) \times C_{(\mathrm{NaOH})}}{M \times (1 - X)} \quad (1)$$

$$X = \frac{m_2 - m_1}{m_2} \times 100 \quad (2)$$

where Q (mmol g^{-1}) is the content of sulfonic acid group. V_1 (mL) and V_2 (mL) are the volume of NaOH solution consumed in the blank titration and titrating the exchange effluent,

respectively. $C_{(NaOH)}$ (mol L^{-1}) is the concentration of the standard NaOH solution. M (g) is the mass of the experimental sample. X is the water content of the sodium-form sulfonated polymer. m_1 and m_2 are the mass of the dry and wet polymer, respectively.

4.5 Adsorption experiment

4.5.1 Batch adsorption. 0.01 g of adsorbent was placed into 10 mL of a Cr(III) solution with a specific concentration. The mixture was shaken at 220 rpm and 25 °C for 48 h. After adsorption, the supernatant was diluted in a predetermined ratio, and the concentration of Cr(III) in the treated solution was measured using an ICPE-9000.

4.5.2 Regeneration. After the adsorption experiment, the polymer was recovered by vacuum filtration and subjected to desorption treatment using a 20% sulfuric acid solution under agitation for 24 h. Residual desorption solution was removed from the polymer, followed by rinsing with deionized water and drying the polymers. The regenerated polymer was then reused in the next cycle of the adsorption experiment.

4.5.3 Adsorption–recrystallization. The sulfonated polymer was packed into a chromatography column and initially rinsed with ultra-pure water until the effluent became clear. Subsequently, it was eluted with 1 M HCl until the effluent pH reached 1–2, followed by soaking for 8 h. The polymer was then rinsed with ultra-pure water until the pH reached 5–6, followed by elution with 1 M tetramethylammonium (TMAH) solution until the pH reached 12–14 and soaking for 8 h. Finally, it was rinsed with ultra-pure water until the pH reached 8–9, and the entire procedure was repeated until the effluent metal ion content fell below 1 ppb.

H_3tci was loaded into a PFA adsorption reactor and mixed with ultra-pure water and G3-grade 1 M TMAH solution, along with the pretreated sulfonated polymer. The mixture was subjected to adsorption at 60 °C for 48 h at constant temperature. After adsorption, the solution was immediately filtered, and the filtrate was transferred to a PTA crystallization reactor. A specified amount of G3-grade nitric acid was added, and the solution was programmatically cooled to 5 °C and held at that temperature for 4 h. The resulting solids were filtered, rinsed three times with ultra-pure water and once with G3-grade isopropanol, and then dried to obtain purified H_3tci. For Cr(III) concentration analysis, 0.2 g of the purified product was dissolved in 200 g of water and analyzed by ICP-MS.

4.6 Calculation

4.6.1 Adsorption capacity and removal rate. The adsorption capacity Q_e (mg g^{-1}) and the removal rate R_e (%) of Cr(III) at equilibrium were calculated as follows:

$$Q_e = C_0 - C_e \times V/m \tag{3}$$

$$R_e = \frac{C_0 - C_e}{C_0} \times 100\% \tag{4}$$

where C_0 (mg L^{-1}) is the initial concentration of Cr(III), C_e (mg L^{-1}) is the equilibrium concentration of Cr(III), V (mL) is the total volume of the solution and m is the mass of the adsorbent.

4.6.2 Adsorption kinetics. 1) Pseudo-first-order kinetic model

$$\ln(Q_e - Q_t) = \ln Q_e - k_1 t \tag{5}$$

2) Pseudo-second-order kinetic model

$$\frac{t}{Q_t} = \frac{1}{k_2 {Q_e}^2} + \frac{1}{Q_e} t \tag{6}$$

where Q_e (mg g^{-1}) and Q_t (mg g^{-1}) are the adsorption capacity of the adsorbent at the contact time t (min) and equilibrium time, respectively. k_1 (min^{-1}) and k_2 (g mg^{-1} min^{-1}) are the adsorption rate constant of the pseudo-first-order and pseudo-second-order, respectively.

3) Weber–Morris model

$$Q_t = k_i t^{1/2} + c_i \tag{7}$$

where k_i is the intraparticle diffusion constant, and c_i is the thickness of the boundary layer.

4.6.3 Adsorption isotherm. 1) Langmuir model

$$\frac{C_e}{Q_e} = \frac{1}{Q_m K_L} + \frac{C_e}{Q_m} \tag{8}$$

2) Freundlich model

$$\ln Q_e = \frac{1}{n} \ln C_e + \ln K_F \tag{9}$$

where Q_m (mg g^{-1}) and Q_e (mg g^{-1}) are the maximum and equilibrium adsorption capacity of the adsorbent, respectively. C_e (mg L^{-1}) is the equilibrium concentration. K_L (L mg^{-1}) and K_F (mg g^{-1} (L $mg^{-1})^{1/n}$) are the equilibrium constant of the Langmuir model and Freundlich model, respectively. n is the constant related to the adsorption intensity.

4.6.4 Thermodynamics

$$K_d = \frac{Q_e}{C_e} \tag{10}$$

$$\Delta G = -RT \ln K_d \tag{11}$$

$$\Delta G = \Delta H - T\Delta S \tag{12}$$

$$\ln K_d = \frac{\Delta S}{R} - \frac{\Delta H}{RT} \tag{13}$$

where K_d is the thermodynamic equilibrium constant. Q_e (mg g^{-1}) is the adsorption capacity of the equilibrium. C_e (mg L^{-1}) is the concentration of the equilibrium. ΔG (kJ mol^{-1}) is the Gibbs free energy change. R (8.314 J mol^{-1} K^{-1}) is the

thermodynamic constant. T (K) is the temperature. ΔH (kJ mol^{-1}) is the standard enthalpy change. ΔS (kJ mol^{-1} K^{-1}) is the standard entropy change.

Data availability

The data that support the findings of this study are available from the corresponding author upon reasonable request.

Author contributions

Huiyao Huang: conceptualization, data curation, investigation and writing – original draft; Shiquan Zhong: formal analysis, investigation, software, data curation and methodology; Yawen Chen: investigation and validation; Wangquan Gong: software and validation; Changshen Ye: formal analysis and validation; Ting Qiu: project administration, resources, supervision and funding acquisition; Jie Chen: supervision, resources and writing – review & editing.

Conflicts of interest

The authors declare no conflicts of interest.

Acknowledgements

This work was supported by the National Natural Science Foundation of China (Grant No. 22478077, 22278077). We also greatly acknowledge support from the State Key Laboratory of Green and Efficient Development of Phosphorus Resources.

References

1 Z. Liu, Q. Liu, X. Ren, J. Xie, N. Chang and Q. Zhang, Novel photobase generators mediated thiol-epoxy "click" reaction for self-healing, degradable and recyclable photoresist based on bio-vanillin and eugenol, *Chem. Eng. J.*, 2025, **503**, 158304.
2 Q. Wang, C. Yan, F. You and L. Wang, A new type of sulfonium salt copolymers generating polymeric photoacid: Preparation, properties and application, *React. Funct. Polym.*, 2018, **130**, 118–125.
3 Y. Liu, J. Wang and W. Li, Achieving less than 100 ppb total metal ion concentration in ESCAP resins synthesized by atom transfer radical polymerization, *Macromol. Mater. Eng.*, 2024, **309**, 2300418.
4 V. Vlnieska, A. Mikhaylov, M. Zakharova, E. Blasco and D. Kunka, Epoxy resins for negative tone photoresists, *Polymer*, 2019, **11**, 1457.
5 Y. Ding, Y. Xin, Q. Zhang and Y. Zou, Acrylic resins with oxetane pendant groups for free radical and cationic dual-curing photoresists, *Mater. Des.*, 2022, **213**, 110370.
6 Z. Tang, X. Guo, H. Wang, H. Chen and W. Kang, A new metallization method of modified tannic acid photoresist patterning, *Ind. Chem. Mater.*, 2024, **2**, 284–288.
7 M. Y. Zhang, G. X. Zhang, J. Q. Gao and Z. B. Han, A 1D linear chain coordination polymer constructed by Cu(II) with H_3Tci and Bipy ligands (H_3Tci = tris(2-carboxyethyl) isocyanurate, Bipy = 4,4′-bipyridine), *Russ. J. Coord. Chem.*, 2012, **38**, 279–283.
8 X. Sun, Y. Wang, Y. Tang, B. Zhang, W. Wei, X. Li, X. Fei and X. Liu, Synthesis of isocyanurate-based imidazole carboxylate as thermal latent curing accelerator for thermosetting epoxy resins, *J. Appl. Polym. Sci.*, 2020, **137**, 49221.
9 Q. Liu, Z. Li, B. Liu and H. Sun, A new melt crystallization process for efficient purification of chlorobromobenzene, *Sep. Purif. Technol.*, 2020, **251**, 117367.
10 Y. Song, T. Gotoh and S. Nakai, Simultaneous removal of anionic and cationic species by ionic hydrogels via positively charged complex: adsorption mechanism of arsenic(V) and chromium(III) in highly acidic system, *ACS ES&T Water*, 2024, **4**, 2005–2017.
11 W. Liu, Y. Liu, Z. Yuan and C. Lu, Recent advances in the detection and removal of heavy metal ions using functionalized layered double hydroxides: a review, *Ind. Chem. Mater.*, 2023, **1**, 79–92.
12 C. Darmali, S. Mansouri, N. Yazdanpanah, Z. K. Nagy and M. W. Woo, Continuous lactose recovery from acid whey by mixed suspension mixed product removal (MSMPR) crystallizer in the presence of impurities, *Chem. Eng. Process.*, 2022, **180**, 108752.
13 E. Kassahun, J. Fito, S. Tibebu, T. T. I. Nkambule, T. Tadesse, T. Sime and H. Kloos, The application of the activated carbon from cordia africana leaves for adsorption of chromium(III) from an aqueous solution, *J. Chem.*, 2022, **2022**, 4874502.
14 S. Parambadath, A. Mathew, A. Mohan and C.-S. Ha, Chelation dependent selective adsorption of metal ions by Schiff Base modified SBA-15 from aqueous solutions, *J. Environ. Chem. Eng.*, 2020, **8**, 104248.
15 S. Panja, S. Hanson and C. Wang, EDTA-inspired polydentate hydrogels with exceptionally high heavy metal adsorption capacity as reusable adsorbents for wastewater purification, *ACS Appl. Mater. Interfaces*, 2020, **12**, 25276–25285.
16 B. Gupta, A. Deep and S. N. Tandon, Recovery of chromium and nickel from industrial waste, *Ind. Eng. Chem. Res.*, 2002, **41**, 2948–2952.
17 B. L. Rivas, M. Jara and E. D. Pereira, Preparation and adsorption properties of the chelating resins containing carboxylic, sulfonic, and imidazole groups, *J. Appl. Polym. Sci.*, 2003, **89**, 2852–2856.
18 H. Wang, T. Wang, R. Ma, K. Wu, H. Li, B. Feng, C. Li and Y. Shen, Facile synthesis of sulfonated covalent organic framework for the adsorption of heavy metal ions, *J. Taiwan Inst. Chem. Eng.*, 2020, **112**, 122–129.
19 J. Liu, Y. Chen, S. Jiang, J. Huang, Y. Lv, Y. Liu and M. Liu, Rapid removal of Cr(III) from high-salinity wastewater by cellulose-g-poly-(acrylamide-co-sulfonic acid) polymeric bio-adsorbent, *Carbohydr. Polym.*, 2021, **270**, 118356.
20 L. Dewa, S. M. Tichapondwa and W. Mhike, Adsorption of hexavalent chromium from wastewater using polyaniline-

coated microcrystalline cellulose nanocomposites, *RSC Adv.*, 2024, **14**, 6603–6616.
21 F. Zhang, L. Xi, M. Zhao, Y. Du, L. Ma, S. Chen, H. Ye, D. Du and T. C. Zhang, Efficient removal of Cr(VI) from aqueous solutions by polypyrrole/natural pyrite composites, *J. Mol. Liq.*, 2022, **365**, 120041.
22 R. Castaldo, G. Gentile, M. Avella, C. Carfagna and V. Ambrogi, Microporous hyper-crosslinked polystyrenes and nanocomposites with high adsorption properties: A review, *Polymer*, 2017, **9**, 651.
23 Y. Chen, M. He, C. Wang and Y. Wei, A novel polyvinyltetrazole-grafted resin with high capacity for adsorption of Pb(II), Cu(II) and Cr(III) ions from aqueous solutions, *J. Mater. Chem. A*, 2014, **2**, 10444–10453.
24 T. Chen, T. Da and Y. Ma, Reasonable calculation of the thermodynamic parameters from adsorption equilibrium constant, *J. Mol. Liq.*, 2021, **322**, 114980.
25 E. C. Lima, A. Hosseini-Bandegharaei, J. C. Moreno-Piraján and I. Anastopoulos, A critical review of the estimation of the thermodynamic parameters on adsorption equilibria. Wrong use of equilibrium constant in the Van't Hoof equation for calculation of thermodynamic parameters of adsorption, *J. Mol. Liq.*, 2019, **273**, 425–434.
26 M. e. A. Zennaki, L. Tennouga, B. Bouras, C. Benouis, G. B. Stambouli and N. Benzemra, Comparison of three materials derived from waste EPS for heavy metal removal efficiency, *Water, Air, Soil Pollut.*, 2023, **235**, 31.
27 Y. Zang, Y. Yu, Y. Chen, M. Fan, J. Wang, J. Liu, L. Xu, H. Jia and S. Dong, Synthesis of conjugated microporous polymers rich in sulfonic acid groups for the highly efficient adsorption of Cs^+, *Chem. Eng. J.*, 2024, **484**, 149709.
28 A. P. da Luz Corrêa, P. M. M. da Silva, M. A. Gonçalves, R. R. C. Bastos, G. N. da Rocha Filho and L. R. V. da Conceição, Study of the activity and stability of sulfonated carbon catalyst from agroindustrial waste in biodiesel production: Influence of pyrolysis temperature on functionalization, *Arabian J. Chem.*, 2023, **16**, 104964.
29 Y. Sun, J. Zhao, J. Wang, N. Tang, R. Zhao, D. Zhang, T. Guan and K. Li, Sulfur-doped millimeter-sized microporous activated carbon spheres derived from sulfonated poly(styrene–divinylbenzene) for CO_2 Capture, *J. Phys. Chem. C*, 2017, **121**, 10000–10009.
30 Y. Liu, M. Shi, S. Fang, Q. Zhang, Q. Wu, N. Li and D. Lin, Superoleophobic hierarchical honeycomb hydrogels for effective heavy metal removal in crude oil emulsion, *ACS Appl. Mater. Interfaces*, 2025, **17**, 16187–16201.
31 T. d. F. Neves, C. B. Lopes, V. R. Mastelaro, R. F. Dantas, C. M. Silva and P. Prediger, Toxic metals removal by new membranes based on graphene oxide and a cationic polymer: Influence of chemical and morphological aspects, *Chem. Eng. J.*, 2024, **498**, 155496.
32 K. Jahan, D. Thankachan, K. Shakya, N. Mehrotra, C. S. Nimish and V. Verma, Removal of heavy metal ions (Pb^{2+}, Cu^{2+}, Cr^{3+}, and Cd^{2+}) from multimetal simulated wastewater using 3-aminopropyl triethoxysilane grafted agar porous cryogel, *Int. J. Biol. Macromol.*, 2024, **282**, 136784.
33 D. Tang, M. Yin, X. Du, Y. Duan, J. Chen and T. Qiu, Wettability tunable conjugated microporous poly(aniline)s for long-term, rapid and ppb level sequestration of Hg(II), *Chem. Eng. J.*, 2023, **474**, 145527.
34 J. Wang and X. Guo, Adsorption isotherm models: Classification, physical meaning, application and solving method, *Chemosphere*, 2020, **258**, 127279.
35 E. Majigsuren, U. Byambasuren, M. Bat-Amgalan, E. Mendsaikhan, N. Kano, H. J. Kim and G. Yunden, Adsorption of chromium(III) and chromium(VI) ions from aqueous solution using chitosan–clay composite materials, *Polymer*, 2024, **16**, 1399.
36 W. Zhang, X. Ma, R. Li, W. Yang, Q. Li, X. Sun, J. Li and J. Shen, Rapid sequestration of chelated Cr(III) by ferrihydrite: Adsorption and overall transformation of Cr(III) complexes, *Colloids Surf., A*, 2021, **625**, 126819.
37 X. Gu, P. Guo, Z. Li, X. Xu, Y. Cao, G. Yang, C. Kuang, X. Li, Y. Qing and Y. Wu, A multifunctional coconut shell biochar modified by titanium dioxide for heavy metal removal in water/soil and tetracycline degradation, *J. Cleaner Prod.*, 2024, **482**, 144192.
38 P. Thamarai, V. C. Deivayanai, P. Swaminaathan, S. Karishma, A. Saravanan, A. S. Vickram and P. R. Yaashikaa, Experimental investigation of Cd(II) ion adsorption on surface-modified mixed seaweed biosorbent: A study on analytical interpretation and thermodynamics, *Environ. Res.*, 2024, **260**, 119670.
39 D. H. Mir and M. A. Rather, Kinetic and thermodynamic investigations of copper(II) biosorption by green algae Chara vulgaris obtained from the waters of Dal Lake in Srinagar (India), *J. Water Process Eng.*, 2024, **58**, 104850.
40 J. Di, Z. Ruan, S. Zhang, Y. Dong, S. Fu, H. Li and G. Jiang, Adsorption behaviors and mechanisms of Cu^{2+}, Zn^{2+} and Pb^{2+} by magnetically modified lignite, *Sci. Rep.*, 2022, **12**, 1394.
41 J. Wang and X. Guo, Adsorption kinetic models: Physical meanings, applications, and solving methods, *J. Hazard. Mater.*, 2020, **390**, 122156.
42 Z.-H. Yang, S. Xiong, B. Wang, Q. Li and W.-C. Yang, Cr(III) adsorption by sugarcane pulp residue and biochar, *J. Cent. South Univ.*, 2013, **20**, 1319–1325.
43 A. T. K. Tran, T. T. Pham, Q. H. Nguyen, N. T. T. Hoang, D. T. Bui, M. T. Nguyen, M. K. Nguyen and B. Van der Bruggen, From waste disposal to valuable material: Sulfonating polystyrene waste for heavy metal removal, *J. Environ. Chem. Eng.*, 2020, **8**, 104302.